

CAAP Annual Report

Date of Report: July 11, 2016

Contract Number: DTPH5614HCAP03

Prepared for: Government Agency: DOT

Project Title: Experimental Characterization and Monitoring of Early Stage Corrosion
Degradation of Pipeline Steels

Prepared by: Iowa State University

Contact Information: Professor Ashraf Bastawros,
T.A. Wilson Professor of Engineering and Associate Chair for Resrach,
Department of Aerospace Engineering
2271 Howe Hall, Rm 1200
Ames, IA 50011-2271
Phone: 515-294-3039 Fax: 515-294-3262
Email: bastaw@iastate.edu

For quarterly period ending: March 31, 2016

Business and Activity Section

(a) Generated Commitments - None to report

(b) Status Update of Past Quarter Activities - The main objective of the proposed work is to enhance the pipeline safety through understanding the early corrosion mechanisms in high strength pipeline steels that lead to stress corrosion cracking with a focus on measurable degradation parameters that can guide the development of advanced NDE measurement procedures.

The focus of this quarter was to, (i) estimate the extent of the subsurface damage due to the corrosion process. Since the surface was cover by chemical product from the electrochemical corrosion process, we developed a procedure to remove these deposited corrosion product layer, without disturbing the near surface layer of the material. The cleaned surface was examined by scanning electron microscope to identify the residual phases on the surface. A combined dynamic and quasi-static nano-indentation testing protocol was implemented to examine the near-surface damage evolution on the cleaned corroded surface. And (ii), identify the nature of the residual stress builds up during the early stage of the corrosion process. Within the experimental observation window, we have identified the following major aspect for the early stage of SCC:

1. Electrochemical corrosion process starts aggressively, forming corrosion products (iron oxides). As the oxides thicken, iron transport is impeded, while the electrochemical ohmic

resistance is increased. These combined processes greatly reduce the rate of the corrosion process.

2. The electrochemical corrosion process has resulted in a soft layer near the surface with lower hardness (or flow stress). The nano-probe measurements showed about 20% drop in hardness, with no measureable changes in the elastic modulus. Our speculation is that the corrosion process has generated excessive atomic vacancies that is responsible for such drop.

b.1 Removal of Corrosion Product Layer by Acetic Acid Treatment:

In the previous reports, we have showed that the corrosion products are being precipitated on the surface. We have previously employed Clarke's solution to remove the corrosion products and render a clean surface for nanoindentation measurements. We have found that Clarke's solution chemically affects the sample surface and degrades the near surface properties, in the absence of corrosion. The summary of the mechanical analysis of different surface treatments are shown in Fig. 1 for X-70 steel samples. Figure 1(a) shows the indentation modulus as a function of indent depth for the base sample (pristine surface with no treatment or corrosion), and a pristine surface treated by Clarke's solution. As can be clearly seen, the indentation modulus can be decreased by up to %100 by application of Clarke's solution on the surface, and extend to a depth of 0.5-1 μm . The optical micrographs of the exposed surface Clarke's solution (Fig. 1(c)) show visible deterioration and evolution of additional roughness.

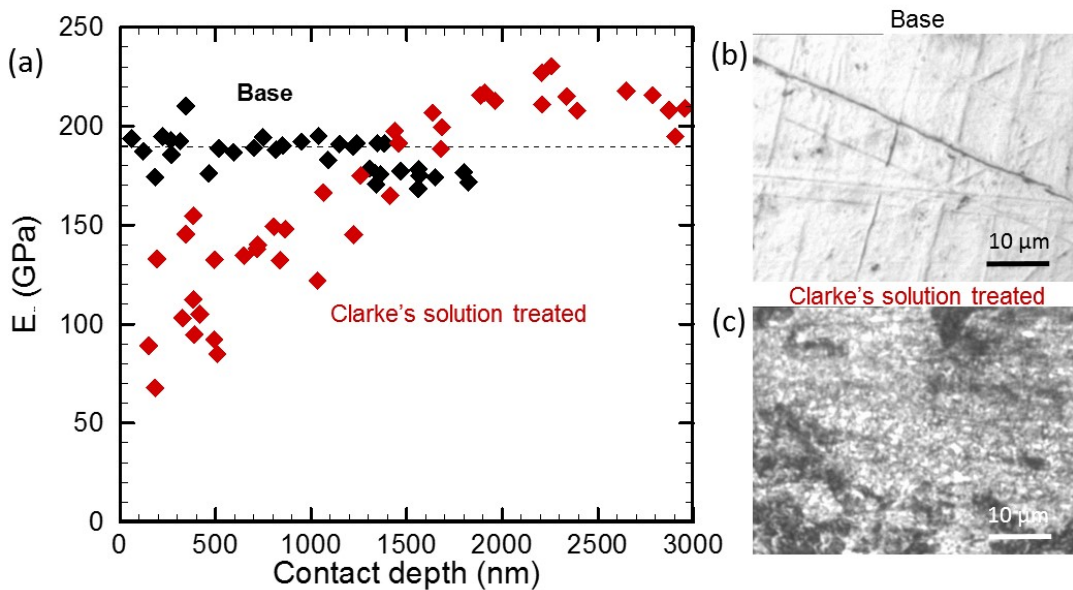


Figure 1: (a) Indentation modulus as a function of indent depth for pristine surface (black) and Clarke's solution treated surface (red). (b, c) Optical micrographs of surfaces before the indentation. Solution treated surface shows many morphological evolutions.

Accordingly, we have examined a wide range of cleaning agents and identified acetic acid as one of the least damaging to the subsurface layer. The proper surface cleaning would entail soaking the corroded sample in a diluted solution (0.1M) of acetic acid for 5-8 min, then cleaning the by deionized water and methanol. Figure 2 shows the SEM images of the sample surface after the corrosion process, and after the cleaning process. The corroded sample exhibited a product layer Fig 2(a) with roughness arising from the sedimentation and redistribution of the dissolved corrosion products. The pattern of mud cracking arises from the drying process. Though, none of these features has direct correlations to the underlying micro-structure. Figure 2 (b, c) shows the surface texture after the cleaning process. The granular texture can be clearly identified. The average grain size is in the range of 5-10 μm . Additionally, extensive GB grooving can be seen with width of about 100-300nm on the surface.

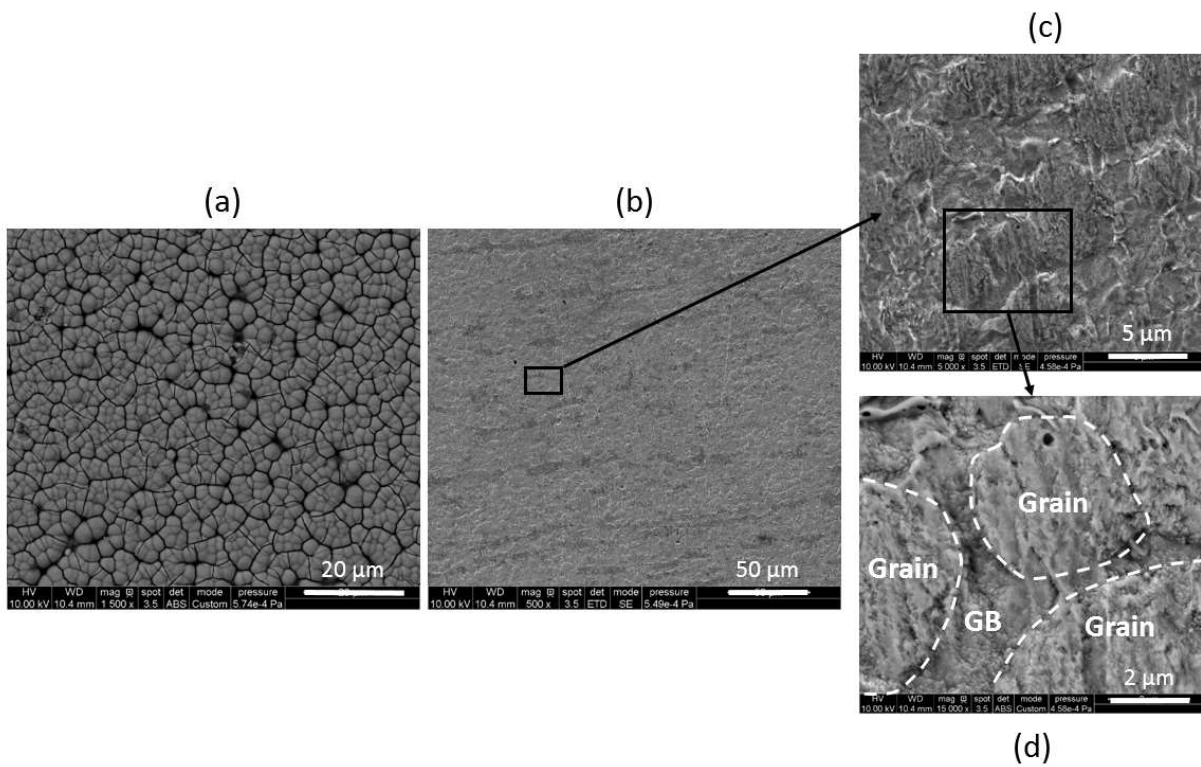


Figure 2: SEM micrographs showing (a) X70 steel surface after the corrosion experiment for 120 min at a constant peak potential of -0.5V/SCE in bicarbonate solution (1M NaHCO_3), (b) the cleaned corroded surface for 8 min in diluted acetic acid. (c, d) Higher magnification SEM images of the surface, showing excessive grain boundary grooving.

b.2 Measurement of Near-surface Mechanical Properties by Nano-indentation:

Characterization of near surface damage was conducted by high resolution dynamic nanoindentation technique employing Hysitron nanoDMA[®] III transducer with 90° cube corner indenter tip. The load profiling profile has a superimposed small oscillatory dynamic force during each loading step, which facilitates the continuous measurement of the near surface mechanical

response. The methodology for data analysis, proposed by Oliver and Pharr (1992) [1], was utilized in determining the indentation hardness, H , and modulus, E .

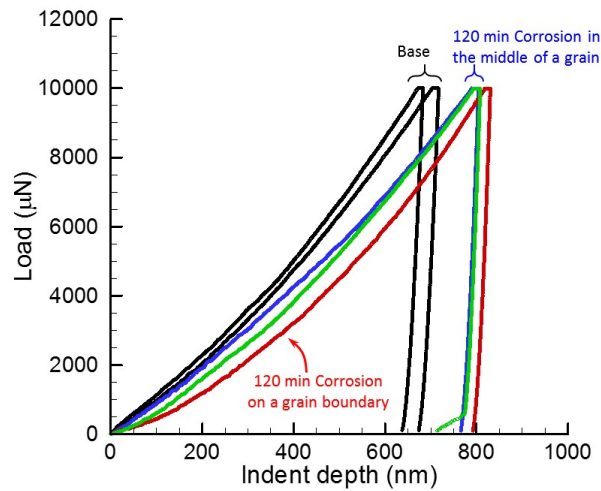


Figure 3: Force-indentation depth curves on the base (prestine with no corrosion, black) and the 120 min corroded samples (colored) after removing the chemical products. A consistent softer response can be seen for the corroded surfaces.

A set of dynamic nanoindentation experiments was performed on the surface of the sample 120 min exposure time, after the corrosion product layer was removed by 0.1M acetic acid solution. All the indentations were performed within the middle of grain. Figure 3 shows force-indentation depth curves for the base (black curves) sample, and 120 min corroded sample after the cleaning (color curves). A consistent softer response can be seen for the corroded surface. Though, the initial loading segment was almost the same for the reference and the corroded sample, until reaching an indentation depth of about 400nm. Then, the slope of the loading curves diverges. The maximum indentation depth is about 100nm deeper for the corroded surface under the same applied load. The indent on a grain boundary was consistently softer.

Figures 4 shows the variation of the continuously measured E , and H as a function of indent depth. Within the experimental error, there is noticeable difference in the measurements of the modulus for the corroded and the base material. The red curve corresponds to an indentation on a grain boundary and exhibiting an initial compliant response with $E \sim 75\%$ of that of the other experiments on either the center of the corroded grain or the reference material. Though an exact value cannot be directly assessed as the measurements near a grain boundary is the convolution of the softer GB response and its thickness [2]. The measured hardness exhibit many unique features. First, the continuous decay of H for the base material until reaching a steady state level is a direct manifestation of the size dependent response in this range of measurements. Second, the measured H is consistently lower for the corroded surface. Third, in the corroded samples, a transition can be identified in the measured H until reaching a steady state. This transition can be assessed to estimate a thickness of the softer layer near the surface. This layer is estimated to be around $\sim 400\text{nm}$.

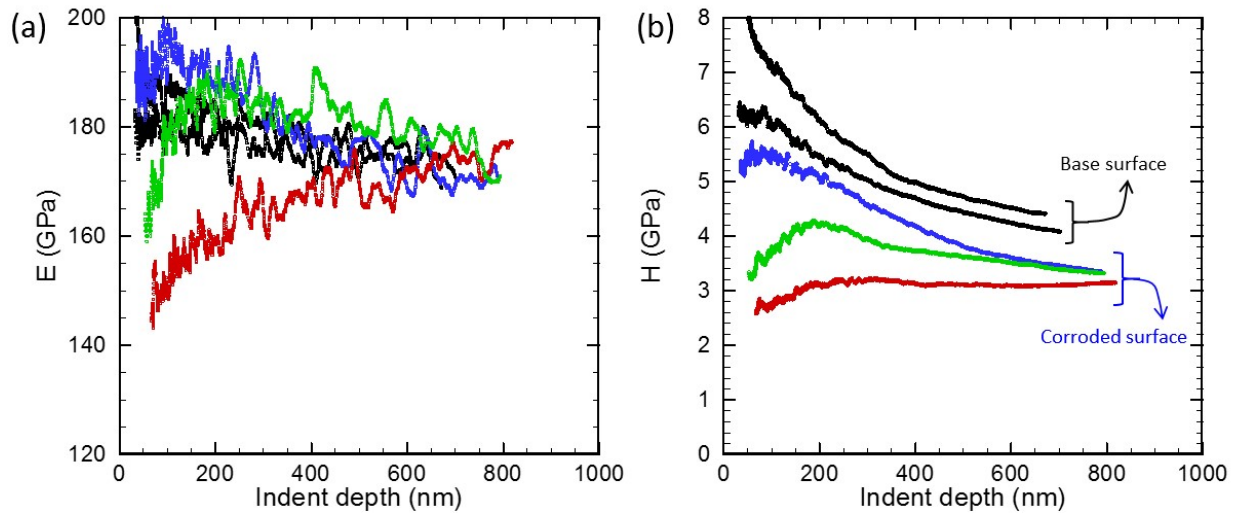


Figure 4: The corresponding indentation (a) modulus and (b) hardness as a function of indent depth for the base (no corrosion, black) and the 120 min corroded samples (colored) after removal of the corrosion product.

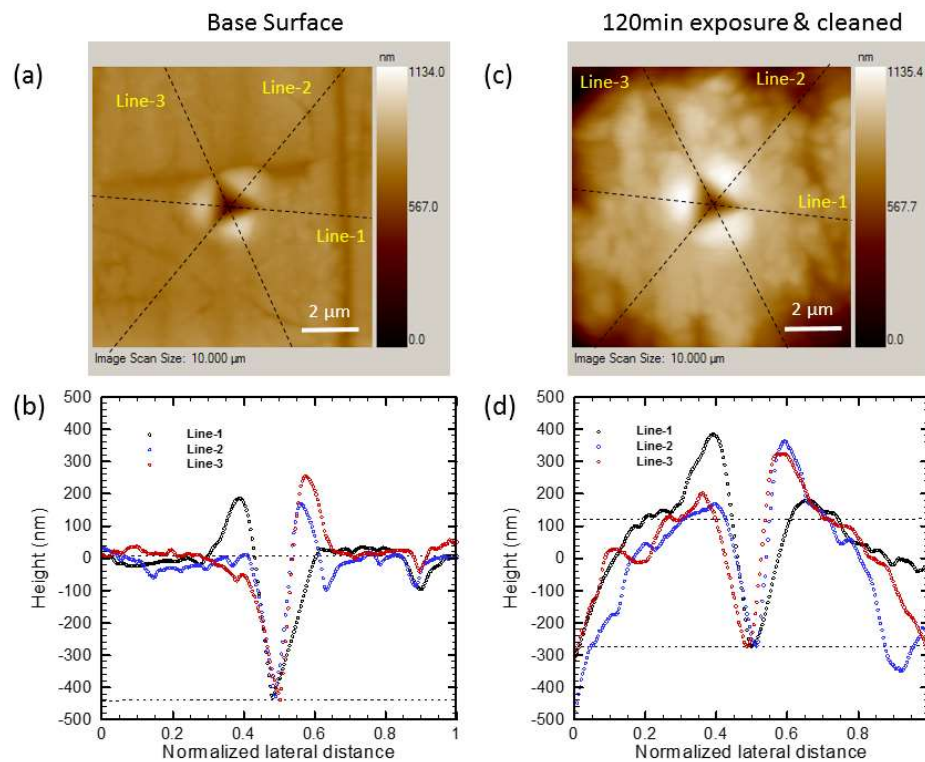


Figure 5: AFM surface scans of the indentation imprints on (a) the base surface with no corrosion, and (b) 120 min corroded sample surfaces. The corresponding height profiles of each line are presented in (c) and (d), respectively, showing a deeper indent for the corroded surface.

Figure 5 shows two atomic force microscope (AFM) scans of indentations on the pristine reference surface and on the corroded surface at the middle of a grain. It can be seen that the indentation on the corroded surface is much deeper by about 50-80nm. This is very contrasting

with the overall force-indentation curves which were about 100nm deeper for the corroded case. This effect will be further explored in the next section.

b.3 Grain Boundary Damage Evolution

The multiple indentation on the center of surface grains highlighted the possibility of softer grain boundaries. To highlight this effect, a set of quasi-static shallow indentation were performed on a line traversing the grain boundary as shown in Fig. 6. The indents were performed under a constant load of 1mN and 1 μ m apart. This range of loading would limit the indentation to the initial sink-in range [2, 3] as well as limiting the indentation process zone to about 500nm. Figure 6(a) is an AFM surface topography rendering of the grain boundaries and the imposed line of the indents. Figure 6(b) is the indentation imprints, shown in the surface gradient mode. The variations of E and H across the GB are shown in Figs. 6(c, d), respectively. There is an obvious drop in both quantities across the GB from those in the middle of the grain. While the drop is about 15-30%, however again the actual GB E and H could be much lower as the measurements is greatly affected by the GB thickness [2]. For a typical GB in the range of 0.1-0.3 μ m, the properties might be reduced by an order of magnitude from their bulk of the grain values due to the corrosion process.

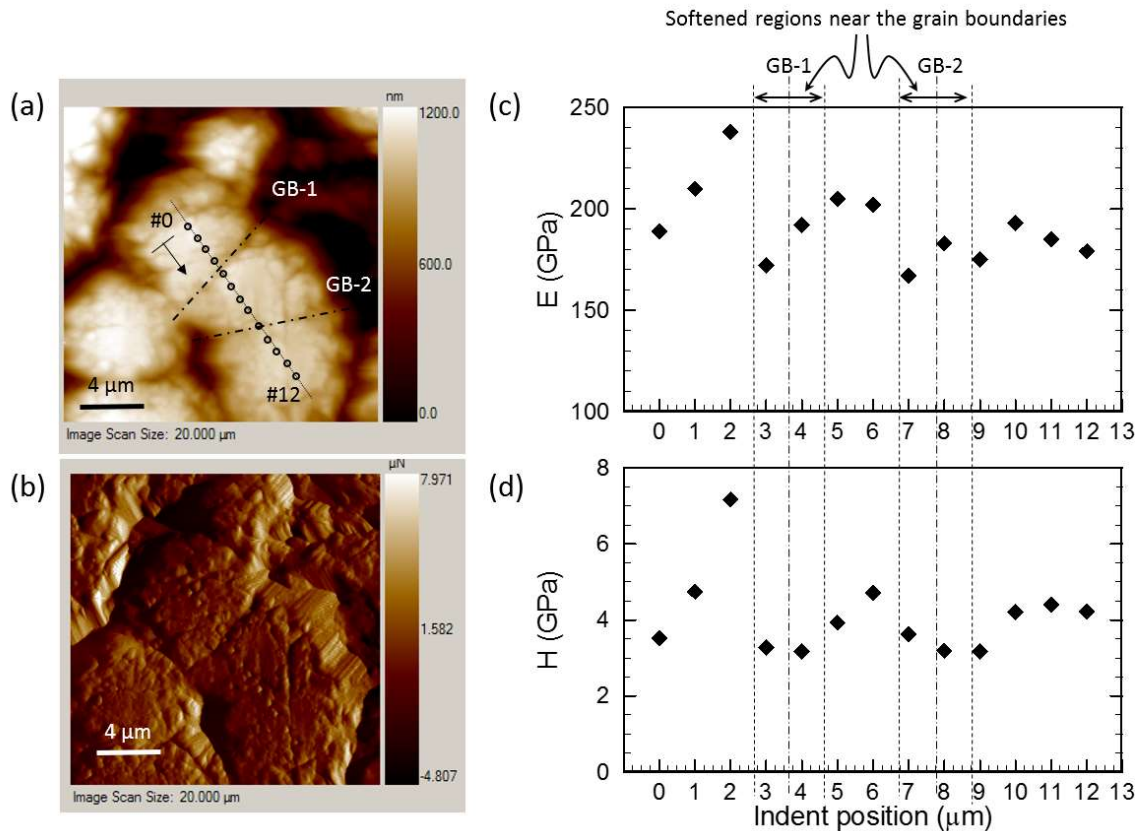


Figure 6: (a) AFM surface topography profile of the corroded and cleaned surface, showing the line of indentation, and GBs. (b) AFM surface gradient showing the line of indent imprints, (c, d) The variation of E and H across the GB, and showing the relative reduction compared to the bulk of the grain.

b.4 In Situ Measurement of Residual Stress Development during the Corrosion Process

During this period, we have focused on repeating the in situ stress measurement experiment under different electrochemical potential to examine the sensitivity of the intergranular corrosion process with the potential. The experiment was conducted on X-70 steel, exposed to bicarbonate solution (1M NaHCO₃) for 120 min. Figure 7 shows the measured residual stress builds up and (dashed lines) and dissolution current density (solid lines) during the electrochemical process. A small tensile stress build-up is observed during the initial cathodic polarization, then a strong overall residual compressive stress builds up during anodic dissolution. Such compressive residual stress is favorable to hinder the growth of further cracking.

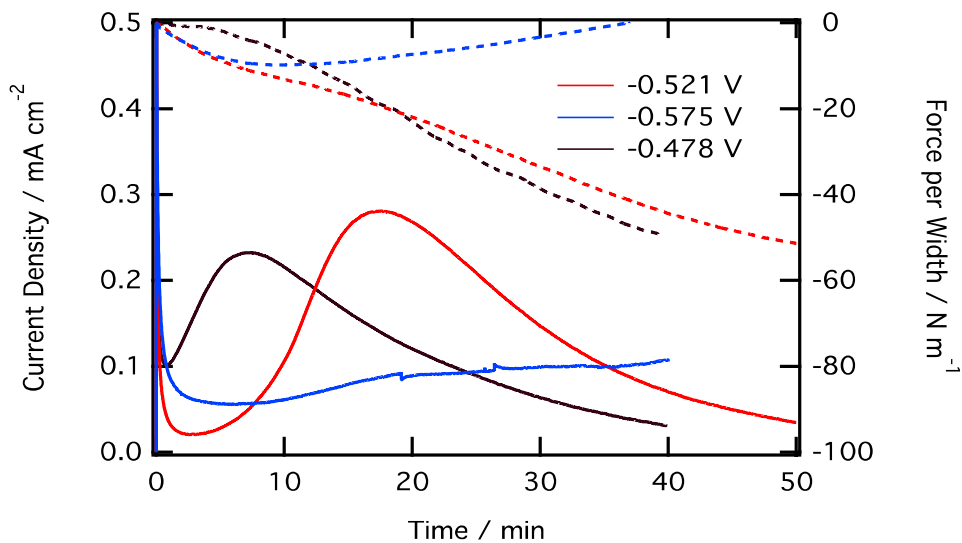


Fig. 7: Measured residual stress builds up (dashed lines) and dissolution current density (solid lines) during the electrochemical process. A small tensile stress build-up is observed during the initial cathodic polarization, then a strong residual compressive stress builds up during anodic dissolution.

(c) Description of any Problems/Challenges –

During this period we have solved a major hurdle associated with existence of the product layer on the surface, which masks the proper evaluation of the near surface damage and mechanical properties. Though the major remaining issue in understanding the physical mechanisms of SCC is understanding the observed strong compressive residual stress. Such compressive stress level as depicted on Fig. 7 should hinder the progression of SCC, though the SEM examination of the surface reveal strong GB grooving. These details are in direct contrast to the nano-indentation measurements, revealing a softening zone near the GB.

(d) **Planned Activities for the Next Quarter** – The main focus of the next phase of work will be on reconciling the electrochemical mechanisms and show how the SCC would further

progress, while generating macroscopic compressive residual stress. Major efforts will be focused on evaluating the progression of the subsurface damage via sectioning and SEM analysis.

(e) References Cited

1. Oliver W.C., Pharr G.M. An Improved Technique for Determining Hardness and Elastic Modulus using Load and Displacement Sensing Indentation Experiments. *Journal of Material Research*, 7, 1564-1583 (1992).
2. Yang, C., Lo, C.T., Narasimhan, B., and Bastawros, A.-F., Measurements of Diffusion Thickness at Polymer Interfaces by Nanoindentation: A Numerically Calibrated Experimental Approach, *Journal of Materials Research*, 24(3), 970-977, (2009).
3. Taljat B., Zacharia T., Pharr G.M., Pile-up behavior of spherical indentations in engineering materials, in *Fundamentals of Nanoindentation and Nanotribology*, edited by Moody N.R., Gerberich W.W., Burnham N., and Baker S.P. (Mater. Res. Soc. Symp. Proc. 522, Warrendale, PA, 1998), p. 33.